Structure of the full-length Shaker potassium channel Kv1.2 by normal-mode-based X-ray crystallographic refinement

Xiaorui Chen[a], Qinghua Wang[b], Fengyun Ni[c], and Jianpeng Ma[a,b,c,1]

[a]Graduate Program of Structural and Computational Biology and Molecular Biophysics, Baylor College of Medicine, One Baylor Plaza, Houston, TX 77030; [b]Verna and Marrs McLean Department of Biochemistry and Molecular Biology, Baylor College of Medicine, One Baylor Plaza, Houston, TX 77030; and [c]Department of Bioengineering, Rice University, Houston, TX 77005

Edited by William N. Lipscomb, Harvard University, Cambridge, MA, and approved April 30, 2010 (received for review January 6, 2010)

Voltage-dependent potassium channels (Kv) are homotetramers composed of four voltage sensors and one pore domain. Because of high-level structural flexibility, the first mammalian Kv structure, Kv1.2 at 2.9 Å, has about 37% molecular mass of the transmembrane portion not resolved. In this study, by applying a novel normal-mode-based X-ray crystallographic refinement method to the original diffraction data and structural model, we established the structure of full-length Kv1.2 in its native form. This structure offers mechanistic insights into voltage sensing. Particularly, it shows a hydrophobic layer of about 10 Å at the midpoint of the membrane bilayer, which is likely the molecular basis for the observed "focused electric field" of Kv1.2 between the internal and external solutions. This work also demonstrated the potential of the refinement method in bringing up large chunks of missing densities, thus beneficial to structural refinement of many difficult systems.

anisotropic *B* factors | ion channel | normal-mode refinement | voltage gating

Voltage-dependent ion channels sense change in the voltage across cell membrane and respond by allowing specific ions in/out with high selectivity and efficiency (1). Among them, voltage-dependent potassium channels (Kv) have been most extensively studied (2–6). In an action potential, the Kv channel allows intracellular potassium getting out of the cell to return the membrane potential to the polarized state, the failure of which could cause overexcitability of neuron cells, leading to neuronal diseases (7, 8). The Kv channel is a homotetramer with four voltage sensors and one central pore domain (9, 10). In each subunit, four transmembrane helices (S1, S2, S3, and S4) make up a voltage-sensor domain, and two transmembrane helices (S5 and S6) contribute to the central pore domain. There are several highly conserved positively charged residues on the S4 helix, the so-called gating charges, which respond to voltage change to open or close the central pore domain (11).

The first mammalian Kv crystal structure was of the Shaker family Kv1.2 from *Rattus norvegicus* [Protein Data Bank (PDB) ID code 2A79], determined to a resolution of 2.9 Å (10). Its structural model was refined by conventional isotropic X-ray crystallographic refinement protocol in CNS (12). Because of the high dynamic and/or static disordering, about 37% of the total molecular mass of the transmembrane portion (residues 131–421) was not resolved. For instance, all the loops connecting S1–S4 helices, and all the side chains on S1 and S3, as well as some of the side chains on S2 and S4, were missing (Fig. 1*A*). In order to obtain a clearer picture of Kv channels, the structure of a "paddle chimera" Kv was recently determined at a higher resolution of 2.4 Å (13). The improvements in the structure were achieved by crystallizing the channel in a lipid environment and by replacing the voltage-sensor paddle of Kv1.2 with the corresponding region of Kv2.1, a closely related Kv channel in the Shab family. Even though the chimera channel behaved similarly to the native Kv1.2 in electrophysiological assays, it is still desirable to have a complete structure for the native Kv1.2 channel.

A normal-mode-based X-ray crystallographic refinement method was recently developed by us and its efficiency in improving structural models was shown in a number of systems such as a supramolecular complex (14), a membrane-bound ion channel (15), a heavily glycosylated protein (16), and other systems (17). The method models anisotropic *B* factors for all atoms by using only a small set of low-frequency normal modes (14, 18, 19). Consequently, the number of parameters used in structural refinement is drastically reduced, which allows a better data-to-parameter ratio, and the structural flexibility is more accurately described than by using conventional isotropic *B*-factor refinement. Therefore, in this study, we employed this refinement method to improve the deposited Kv1.2 structure (PDB ID code 2A79) on the basis of the original diffraction data (10).

Through several iterations of normal-mode-based anisotropic *B*-factor refinement, positional refinement by REFMAC5 and manual model adjustments, we were able to lower the *R* factors and build all the missing atoms in the improved electron density maps. The normal-mode refined structure for Kv1.2 offered insights into the mechanisms of voltage sensing. In particular, a hydrophobic layer of about 10 Å was identified at the midpoint of the membrane bilayer, which is likely the molecular basis for the observed "focused electric field" of Kv1.2 between the internal and external solutions.

Results

Normal-Mode-Based Refinement of Kv1.2 Structure. To eliminate the slight differences in structural statistics because of the use of different structural refinement programs or different versions of them, we generally reminimize the structural models from PDB (14–17). In this study, the Kv1.2 structure (PDB ID code 2A79) (Fig. 1*A*) originally refined by CNS (12) was reminimized using REFMAC5 (20) in CCP4 (21). The reminimization yielded the R_{cryst} factor of 21.9% and R_{free} factor of 24.5%, slightly lower than those for the published model (22.2% for R_{cryst} factor and 25.2% for R_{free} factor) (10). This reminimized model served as the "starting model" in our normal-mode-based refinement.

To start, several parameters for normal-mode-based refinement, including the number of low-frequency modes and the value

Author contributions: J.M. designed research; X.C. and J.M. performed research; X.C., Q.W., F.N., and J.M. analyzed data; and Q.W. and J.M. wrote the paper.

The authors declare no conflict of interest.

This article is a PNAS Direct Submission.

Freely available online through the PNAS open access option.

Data deposition: The structure coordinates of the final Kv1.2 structure have been deposited in PDB with the accession code of 3LUT.

[1]To whom correspondence should be addressed. E-mail: jpma@bcm.tmc.edu.

This article contains supporting information online at www.pnas.org/lookup/suppl/doi:10.1073/pnas.1000142107/-/DCSupplemental.

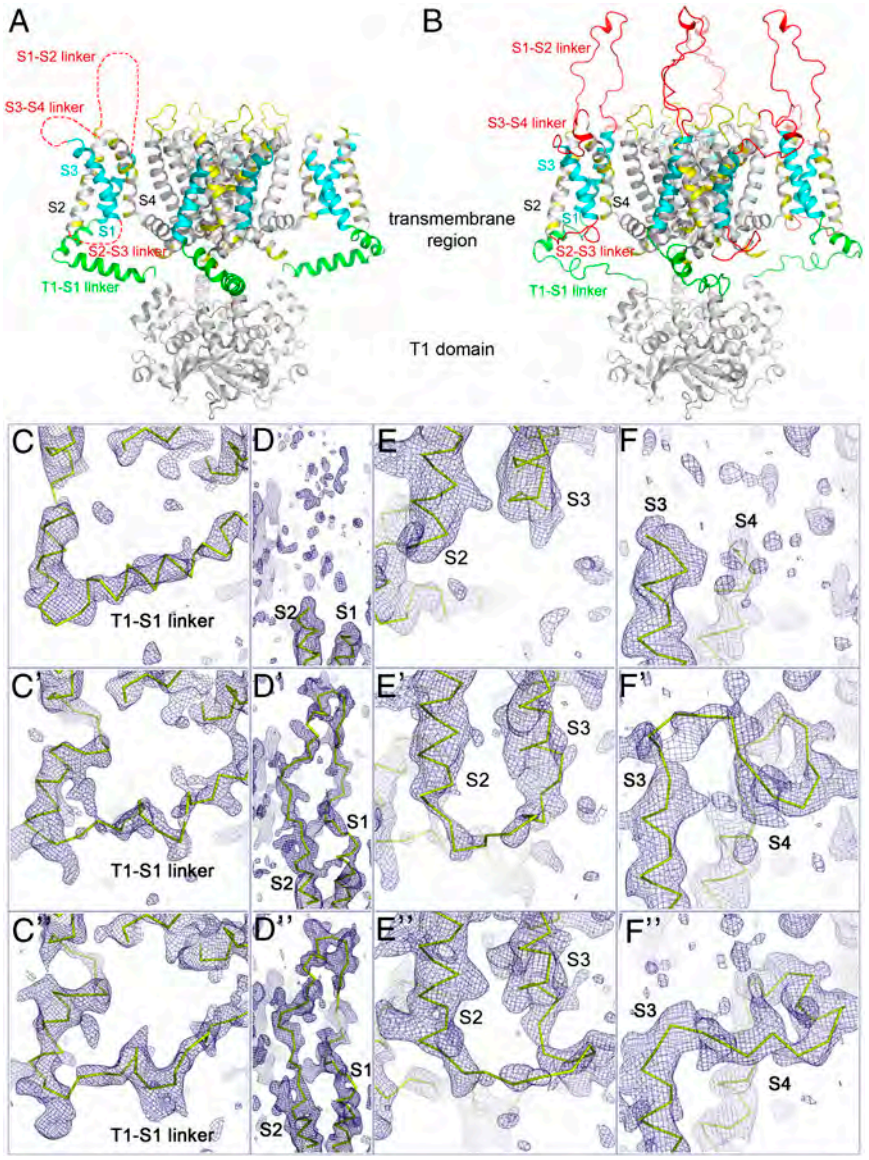

Fig. 1. Overall structural improvements. (*A*) The original Kv1.2 structure (PDB ID code 2A79). (*B*) The final Kv1.2 structure after normal-mode refinement and multicrystal averaging. In both *A* and *B*, red represents the regions newly added, including the S1-S2 linker, S2-S3 linker, and S3-S4 linker; green highlights the T1-S1 linker where large structural adjustments were made and register was determined; cyan suggests the regions (the S1 helix and S3 helix) the registers of which were undetermined in the original Kv1.2 structure but have been fixed in the normal-mode-refined structure; and yellow indicates the rebuilding of the missing side chains on S2 helix, S4 helix, and the linker between S5 and the pore helix. (*C*–*F*′′) Examples of structural improvements in normal-mode refinement comparing the original model (*C*–*F*), the normal-mode model (*C*′–*F*′), and the final model after normal-mode refinement and multicrystal averaging (*C*′′–*F*′′), superimposed with their respective electron density maps. Shown are the T1-S1 linker region (*C*, *C*′, *C*′′), the S1-S2 linker (*D*, *D*′, *D*′′), the S2-S3 linker (*E*, *E*′, *E*′′), and the S3-S4 linker (*F*, *F*′, *F*′′). All maps were $2F_o - F_c$ maps contoured at 0.8σ.

of stiffness, were optimized by running parallel refinements (14–17). We found that 75 modes with stiffness of 30 yielded the lowest R factors. Thus, the number of independent thermal parameters used in the normal-mode refinement was 2,871, representing about 50% reduction in thermal parameters compared with the 4,997 independent thermal parameters for the original model (10). After replacing the isotropic B factors in the starting model with the normal-mode-based anisotropic B factors, the structure was again minimized by REFMAC5, yielding 21.8% for R_{cryst} factor and 24.2% for R_{free} factor, which were slightly lower than those of the starting model (by 0.1% and 0.3% for R_{cryst} and R_{free} factors, respectively).

The normal-mode refinement of Kv1.2 structure converged after a total of six iterative rounds of normal-mode-based anisotropic B-factor refinement, REFMAC5-based positional refinement, and manual adjustments. In each round, guided by the improved composite OMIT $2F_o - F_c$ maps, efforts were made to improve the completeness of the structural model step by step, including building missing main chains and side chains and determining unknown registers (Fig. 1*B*). The normal-mode Kv1.2 structure had 21.2% and 22.3% for R_{cryst} and R_{free} factors, respectively, which were 0.7% and 2.2% lower than those of the starting model (Table S1). There were a total of 851 newly added atoms that were missing in the starting model (Fig. 1*B*), accounting for ~37% of the total mass of the transmembrane portion.

Because of the weak electron density maps for some of newly added loop regions of the transmembrane portion, in order to finalize the coordinates of atoms in these loops with more confidence, we then performed multicrystal averaging between our normal-mode model and the structure of the Kv1.2-Kv2.1 paddle chimera (see *Methods*). The improved phase from multicrystal averaging resulted in small but notable electron density shifts in

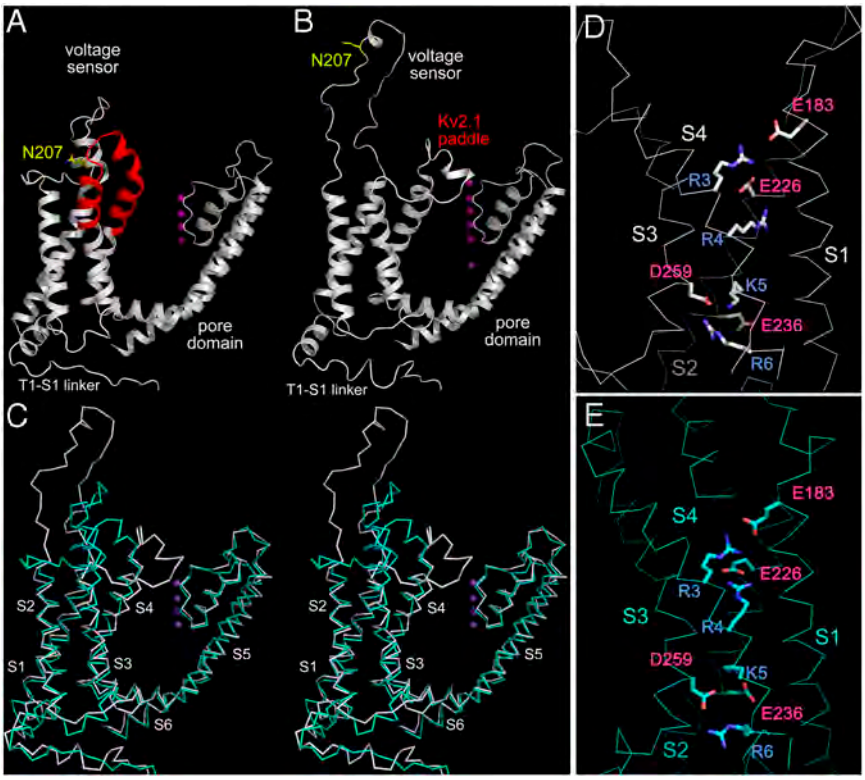

Fig. 2. Comparison of the transmembrane portions of the final Kv1.2 structure and the paddle-chimera structure. (*A*) Ribbon diagram of the paddle chimera structure with the chimera paddle region colored in red. (*B*) Ribbon diagram of the final Kv1.2 structure. The glycosylation site Asn207 (mutated from Gln) in *A* and *B* is highlighted as yellow stick. (*C*) Stereo view of the superposition of transmembrane portion of the final Kv1.2 structure (*White*) and the paddle-chimera structure (*Cyan*). Potassium ions are shown as purple spheres in *A*–*C*. (*D*) The voltage sensors of the final Kv1.2 structure (*White*). (*E*) The voltage sensors of the paddle-chimera structure (*Cyan*). Key residues were shown as sticks for positive gating charges (*Blue*) and their interacting negatively charged residues (*Red*).

some loop regions and the model was finalized accordingly. However, it is important to note that multicrystal averaging between the higher-resolution Kv1.2-Kv2.1 paddle chimera and the original Kv1.2 structure (PDB ID code 2A79) did not bring up the electron density for the interhelix loop regions. Thus, the normal-mode-based refinement method was critical for visualizing those missing loops. The final Kv1.2 model had R_{cryst} and R_{free} factors of 21.1% and 22.1%, which were 0.8% and 2.4% lower than those of the starting model, respectively. The modestly improved R factors, given the ~37% newly added atoms for the transmembrane portion, were probably because of their relatively low contribution to the diffraction data, as a result of structural disordering. The geometry parameters of the final Kv1.2 structure were similar to those of the starting model (Table S1), which made the comparison of R factors before and after the normal-mode-based refinement more robust.

Major Improvements of the Full-Length Kv1.2 Structure. The final full-length Kv1.2 structure had several major improvements over the starting model (Fig. 1). These improvements included: (*i*) the building of the missing main chains and side chains of the S1-S2 linker (35 residues), S2-S3 linker (10 residues), and S3-S4 linker (13 residues); (*ii*) the determination of the registers of T1-S1 linker, S1 helix, and S3 helix; (*iii*) the addition of the missing side chains on S2 helix, S4 helix, and the linker between S5 helix and the pore helix; (*iv*) the retracing of the T1-S1 linker as an extended helix instead of two helices in the original structure. All the structural adjustments were guided by the improved composite OMIT $2F_o - F_c$ electron density maps. Fig. 1 *C*–*F*′′ showed a few examples. In the original structure, the T1-S1 linker was built as two helices (Fig. 1*C*). In the final Kv1.2 structure, it was rebuilt as a random coil (Fig. 1 *C*′ and *C*′′). Moreover, the S1-S2 linker (35 residues) was not built because of the lack of electron density in the original structure (Fig. 1*D*). In the normal-mode refinement, electron density for this region gradually appeared and allowed the building of the full-length S1-S2 linker (Fig. 1 *D*′ and *D*′′). Similarly, the S2-S3 linker (Fig. 1 *E*, *E*′, and *E*′′) and the S3-S4 linker (Fig. 1 *F*, *F*′, and *F*′′) were also built in the newly emerged electron density.

The ability for the normal-mode-based refinement method to result in significant improvement in electron density maps and subsequent substantial model adjustments was probably related to the large phase angle shifts it caused. For instance, the final Kv1.2 differed from the starting model by 15.8° (Fig. S1*a*).

Structural Flexibility of Kv1.2. The fact that a complete model was not possible in the original structure determination suggested that the transmembrane portion of Kv1.2, in particular the voltage-sensor domains, could be highly flexible functionally and/or statically (10). The higher structural flexibility of this portion became very obvious when we compared the *B*-factor profiles of the starting model, the normal-mode model after the first round of normal-mode refinement (Fig. S1*b*), and the final Kv1.2 model (Fig. S1*c*). Although the starting model did show higher *B* factors for the transmembrane region (Fig. S1*b*, *Light Line*), the normal-mode models yielded many more features in *B*-factor profiles (Fig. S1*b*, *Dark Line*; Fig. S1*c*). For instance, the *B*-factor profile of the final Kv1.2 model suggested that all the interhelix regions of the transmembrane portion, including the T1-S1 linker (peak 1), the S1-S2 linker (peak 2), the S2-S3 linker (peak 3), the S3-S4 linker (peak 4), the loop between S5 and the pore helix (peak 5), and the loop between filter region and S6 (peak 6), be of higher mobility than the helices themselves (Fig. S1*c*). Moreover, the regions corresponding to the β-subunit and T1-domain matched very well, indicating the power of the

normal-mode-based method in generating accurate *B*-factor profile with about 50% reduction in thermal parameters.

Comparison with the Paddle Chimera Structure. In the more recent paddle chimera Kv structure solved at 2.4 Å (Fig. 2*A*), the voltage sensor of Kv1.2 was replaced with the corresponding sequence of Kv2.1 (please refer to figure 1*A* in ref. 13 for details of the construct). The replaced region encompassed a total of 32 residues, 27 of which were different from those in Kv1.2 sequence. This region, often referred to as the "voltage-sensor paddle," was comprised of the C-terminal half of S3 (S3*b*), S3-S4 linker, and the N-terminal segment of S4 helix.

We compared the final Kv1.2 model (Fig. 2*B*) and the Kv1.2-Kv2.1 paddle chimera structure (Fig. 2*A*) on the basis of the least-square alignment of S5 and S6 helices, and the superposition was shown in Fig. 2*C*. Overall, the two structures were aligned very well, in particular the transmembrane helices of S1, S2, S4, S5, and S6. As expected from their intrinsic structural flexibility (Fig. S1*c*), large structural differences were noticed at the inter-helix linker regions (Fig. 2*C*). For instance, the N-terminal half of the T1-S1 linker was built as an almost straight polyglycine in the paddle chimera structure, whereas in our final Kv1.2 structure, it was traced as a loop. The 35-residue S1-S2 linker in the chimera structure contained a short helix in the middle to interact with N terminus of the S4 helix (Fig. 2*A*), whereas in our final Kv1.2 structure it was an extended loop (Fig. 2*B*). The different conformations of the S1-S2 linker were probably because of the different S4 helix in these two structures. Previous studies indicated that the middle section of the S1-S2 linker in Kv1.2, including residue 207, can be glycosylated at every position, suggesting that it be fully exposed to external solutions (22, 23). This agreed with the loop conformation of the S1-S2 linker in our final Kv1.2 model (Fig. 2*B*) but was in marked contrast to the more folded conformation of this region in the chimera structure (Fig. 2*A*).

The gating charges R3, R4, K5, and R6 on the S4 helix were all positioned at similar positions between these two structures (Fig. 2 *D* and *E*). In both structures, the gating charges were surrounded by highly conserved negatively charged residues such as E183 (S1) and E226 (S2), E236 (S2), and D259 (S3) (Fig. 2 *D* and *E*). The electrostatic interactions between the gating charges and their surrounding negatively charged partners are believed to be important for voltage gating.

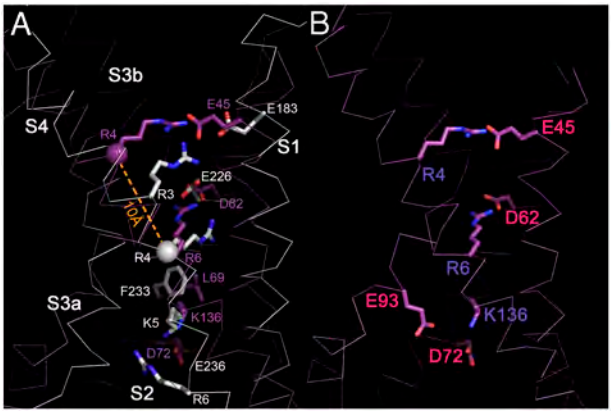

Fig. 3. Comparison of the final Kv1.2 structure and the KvAP structure (PDB ID code 1ORS). (*A*) The superposition of the voltage sensors of the final Kv1.2 structure (*White*) and the KvAP structure (*Purple*). The residues R4 in S4 helix were highlighted with a sphere at its C^{α} atom in two structures, and the distance between them was indicated as a dashed line in orange. (*B*) The charged residues of the voltage sensor in KvAP structure. Key residues were shown as sticks for positive gating charges (*Blue*) and their interacting negatively charged residues (*Red*).

Comparison with the Voltage Sensor of KvAP. The structure of an isolated voltage sensor of a prokaryotic Kv channel, KvAP, was previously determined (9). We compared the structure of voltage-sensor domains of KvAP and our final Kv1.2 model by aligning the S1 and S2 helices (Fig. 3*A*). It was clear that on S1–S3, all the conserved residues aligned very well, including E45 (KvAP) and E183 (Kv1.2) on S1 helix, D62 (KvAP) and E226 (Kv1.2), L69 (KvAP) and F233 (Kv1.2), D72 (KvAP) and E236 (Kv1.2) on S2 helix, E93 (KvAP) and D259 (Kv1.2) on S3 helix. However, S4 helix had rather large relative shifts between these two structures (Fig. 3*A*). Similarly, a large structural shift in S4 helix also existed between the better-quality structure of paddle chimera at 2.4 Å and KvAP. Taken together, these findings suggested that in the architecture of voltage-sensor domains, the S4 helix has the potential to translocate by at least ~10 Å (24).

Similar to those of Kv1.2 and paddle chimera, the gating charges on S4 of KvAP were surrounded by negative charges on other transmembrane helices including E45, D62, D72, and E93 (Fig. 3*B*).

A Hydrophobic Layer in Voltage-Sensor Domain in the Midpoint of the Membrane Bilayer. In the structural study of paddle chimera, a phenylalanine gap at F233 was described (13). In inspecting the voltage-sensor domain of our final Kv1.2 model, we found that near the midpoint of the membrane, there was a layer of 10 Å in thickness formed by ten completely buried residues, V172, I173, S176, I177, and F180 (S1 helix), C229, I230, and F233 (S2 helix), and A262 and I263 (S3 helix) (Fig. 4 and Table 1). Among them, there was one polar residue, S176, and nine hydrophobic residues. Sequence alignment suggested that hydrophobic residues predominate position 176 among other Kv channels (Table 1). Therefore, we collectively referred to this 10 Å-layer as "a hydrophobic layer." This hydrophobic layer was highly conserved among the Kv family (with an overall greater than 90% conservation, except for A262 that is 78% conserved) (Table 1). In the paddle chimera, the same layer of hydrophobic nature was observed (Fig. S2*a*). In KvAP, the hydrophobic layer was composed of residues A34, A35, S38, V39, and V42 (S1 helix), L65, V66, and L69 (S2 helix), A96 and L97 (S3 helix) (Fig. S2*b*). In the middle of this hydrophobic layer, gating charges on S4 [R4 and K5 in Kv1.2 (Fig. 4) and paddle chimera (Fig. S2*a*), R6 and K136 in KvAP (Fig. S2*b*)], and their interacting negatively charged residues from S1–S3 helices (E226 and D259 in Kv1.2 and paddle chimera, D62 and E93 in KvAP) were buried. This thin layer of mostly hydrophobic zone was expected to separate the internal and external solutions to form a focused electric field of ~10 Å (25, 26). Consequently, the gating charges on S4 translocate a much smaller distance than the span of the entire membrane (of up to 30 Å in thickness). It was worth noting that the

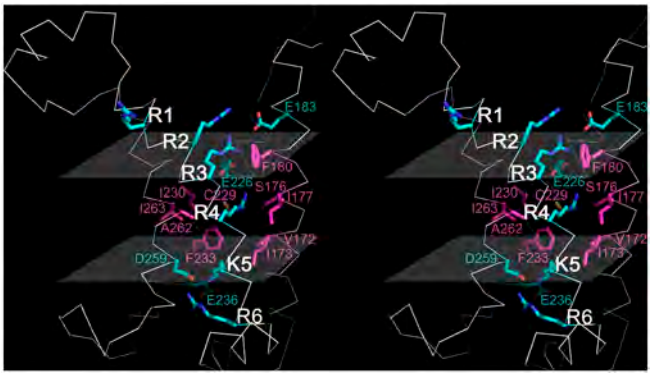

Fig. 4. A hydrophobic layer in the voltage sensor of the final Kv1.2 structure. Hydrophobic residues are colored in magenta and hydrophilic residues in cyan. Transparent planes were drawn at both the upper and lower boundaries of the hydrophobic layer to highlight its thickness.

Table 1. Comparison of solvent accessible surface area and sequence conservation of residues in Kv1.2 and KvAP that are involved in the hydrophobic layer

Residues in Kv1.2	ASA (Å^2)*	Hydrophobic/hydrophilic residues among 250 Kv sequences of the highest homology to Kv1.2	Residues in KvAP	ASA (Å^2)
V172	52	250/0	A34	4
V173	1	249/1	A35	3
S176	7	239/11	S38	5
I177	37	228/22	V39	30
F180	44	227/23	V42	11
C229	6	248/2	L65	16
I230	35	240/10	V66	9
F233	25	250/0	L69	6
A262	5	196/54	A96	8
I263	16	250/0	L97	19

*The accessible surface area (ASA) was calculated by using Areaimol in CCP4 (21).

majority of the hydrophobic core (nine out of ten residues) was from S1 and S2 helices, in agreement with their static role in the gating process to support the large conformational changes carried out by S4 helix (27, 28).

Discussion

Here we report a complete structure of the full-length Shaker family Kv1.2 in its native form based on the original diffraction data (10). This was achieved by using a normal-mode-based X-ray crystallographic refinement method that have been found to be effective in improving structural refinement in a number of biological systems (14–17). In all previous applications, the structural improvement was reflected in building missing side chains, retracing main chains, adding sugar rings, and achieving better fit between the models and the diffraction data (14–17). But in this study, the structural improvement on Kv1.2 was the addition of ~37% molecular mass of the entire transmembrane portion of the channel. Thus, this study highlights the great potential of the refinement method for improving difficult membrane protein structures.

This complete Kv1.2 structure in its native form allows a systematic comparison with previously determined structures of a Kv1.2-Kv2.1 paddle chimera (13) and a prokaryotic Kv channel, KvAP (9). Although the S1–S3 helices were aligned very well among these structures, the gating charges on S4 helix displayed large relative shifts of as much as 10 Å, which suggests that the architecture of voltage-sensor domains be designed in such a way to allow the S4 helix to translocate by at least ~10 Å in voltage gating (24).

Moreover, in the middle of the voltage-sensor domain of the final Kv1.2 structure, we found a hydrophobic layer of 10 Å in thickness formed by ten buried residues (Fig. 4 and Table 1). A further inspection of previously published structures revealed that similar hydrophobic layers also exist in the paddle chimera and in prokaryotic KvAP (Fig. S2), but the biological function of the layer was never discussed. This layer of ~10 Å separates the internal and external solutions and buries inside the gating charges and their interacting negatively charged residues. Previous studies have observed a focused electric field of ~10 Å through which the gating charges on S4 have to travel during voltage gating (25, 26). Thus, the hydrophobic layer that we identified in these three different Kv structures is most likely the molecular basis for such a focused electric field. Interestingly, MacKinnon and colleagues (29) recently described an occluded site formed by F233, E236, and D259 that is located just beneath the hydrophobic layer. Because the current Kv1.2 structure is presumably in an open state and the gating charge R1 in the closed state is probably where K5 is in the open state (29), the closed → open transition of Kv1.2 in gating is expected to involve the transpassing of the gating charges through this focused electric field, accounting for the movement of 3–4 elementary charges per voltage sensors in gating (30–33). The fact that the S1 and S2 helices contribute nine out of ten residues in this hydrophobic layer agrees well with their relative static role in the gating process to support the large conformational changes carried out by S4 helix (27, 28).

Undoubtedly, the electron density maps for Kv1.2 are weaker than those of very well-ordered systems, which is intrinsic to very flexible systems like Kv1.2 at fairly limited resolution without any noncrystallographic symmetry. Although the current normal-mode-based refinement method provided substantial density enhancement, it is unlikely to go beyond the limitation of the original data. In order to demonstrate the level of confidence we had in model building, we also included a $F_o - F_c$ map that was calculated with a region in question removed (in this case the retraced T1-S1 linker highlighted in red was removed) (Fig. S3). The $F_o - F_c$ map contoured at 1.0σ clearly justified our retracing in this region.

Although at the late stage of our refinement a multicrystal averaging was used to further improve the map, it is noteworthy that, without the normal-mode refinement, application of multicrystal averaging alone to the original Kv1.2 model was unable to bring up the large chunks of missing densities. Moreover, the fact that the normal-mode-based refinement can be used in combination with other existing methods emphasizes its versatility in assisting structural refinement of difficult systems.

The effectiveness of normal-mode-based method on refining membrane protein structures is evident in this case and in a previous study of KcsA (15). Part of such a success is probably because of the fact that all membrane proteins are very flexible and crystallized in a nonnative lipid environment so that the crystal structures may slightly deviate from their true native forms. These types of protein structural deformation in the vicinity of native form, regardless of functionally relevant or not, are most likely to follow the trajectory of low-frequency normal modes (34). By offering a better description of such structural deformation, the normal-mode-based method can substantially improve the electron density maps and consequently structural models.

Methods

The procedure of the normal-mode-based refinement was described in previous publications (14, 15). The number of the lowest-frequency modes for generating the best anisotropic *B* factors was 75. At the end of normal-mode-based refinement, multicrystal averaging was performed with DMMULTI program in CCP4 (21) to improve the map by using the known structure of Kv1.2-Kv2.1 paddle chimera channel. The detailed methods are supplied in *SI Materials*.

ACKNOWLEDGMENTS. We gratefully thank Roderick MacKinnon for his insightful comments. J.M. acknowledges support of grants from the National Institutes of Health (R01-GM067801), the National Science Foundation (MCB-0818353), and the Welch Foundation (Q-1512). Q.W. acknowledges support from the National Institutes of Health (R01-AI067839) and a Beginning-Grant-in-Aid award from the American Heart Association (0865186F).

1. Hille B (2001) *Ion Channels of Excitable Membranes* (Sinauer Associates, Sunderland), 3rd Ed.
2. Yellen G (1998) The moving parts of voltage-gated ion channels. *Q Rev Biophys* 31(3):239–295.
3. Tombola F, Pathak MM, Isacoff EY (2005) How far will you go to sense voltage?. *Neuron* 48(5):719–725.
4. Tombola F, Pathak MM, Isacoff EY (2006) How does voltage open an ion channel?. *Annu Rev Cell Dev Biol* 22:23–52.
5. MacKinnon R (2003) Potassium channels. *FEBS Lett* 555(1):62–65.
6. Mackinnon R (2004) Potassium channels and the atomic basis of selective ion conduction (Nobel Lecture). *Angew Chem Int Edit* 43:4265–4277.
7. Pongs O (1999) Voltage-gated potassium channels: From hyperexcitability to excitement. *FEBS Lett* 452(1–2):31–35.
8. Panyi G, Possani LD, Rodriguez de la Vega RC, Gaspar R, Varga Z (2006) K+ channel blockers: Novel tools to inhibit T cell activation leading to specific immunosuppression. *Curr Pharm Design* 12(18):2199–2220.
9. Jiang Y, et al. (2003) X-ray structure of a voltage-dependent K+ channel. *Nature* 423(6935):33–41.
10. Long SB, Campbell EB, Mackinnon R (2005) Crystal structure of a mammalian voltage-dependent Shaker family K+ channel. *Science* 309(5736):897–903.
11. Long SB, Campbell EB, Mackinnon R (2005) Voltage sensor of Kv1.2: Structural basis of electromechanical coupling. *Science* 309(5736):903–908.
12. Brunger AT, et al. (1998) Crystallography & NMR system: A new software suite for macromolecular structure determination. *Acta Crystallogr D* 54(Pt 5):905–921.
13. Long SB, Tao X, Campbell EB, MacKinnon R (2007) Atomic structure of a voltage-dependent K+ channel in a lipid membrane-like environment. *Nature* 450(7168): 376–382.
14. Poon BK, et al. (2007) Normal mode refinement of anisotropic thermal parameters for a supramolecular complex at 3.42-Å crystallographic resolution. *Proc Natl Acad Sci USA* 104(19):7869–7874.
15. Chen X, Poon BK, Dousis A, Wang Q, Ma J (2007) Normal-mode refinement of anisotropic thermal parameters for potassium channel KcsA at 3.2 Å crystallographic resolution. *Structure* 15(8):955–962.
16. Chen X, Lu M, Poon BK, Wang Q, Ma J (2009) Structural improvement of unliganded simian immunodeficiency virus gp120 core by normal-mode-based X-ray crystallographic refinement. *Acta Crystallogr D* 65:633–643.
17. Ni F, Poon BK, Wang Q, Ma J (2009) Application of normal-mode refinement to X-ray crystal structures at the lower resolution limit. *Acta Crystallogr D* 65(Pt 7):633–643.
18. Diamond R (1990) On the use of normal modes in thermal parameters refinement: Theory and application to the bovine pancreatic trypsin inhibitor. *Acta Crystallogr A* 46:425–435.
19. Kidera A, Go N (1990) Refinement of protein dynamic structure: Normal mode refinement. *Proc Natl Acad Sci USA* 87(10):3718–3722.
20. Murshudov GN, Vagin AA, Dodson EJ (1997) Refinement of macromolecular structures by the maximum-likelihood method. *Acta Crystallogr D* 53(Pt 3):240–255.
21. Collaborative Computational Project N (1994) The CCP4 suite: Programs for protein crystallography. *Acta Crystallogr D* 50(Pt 5):760–763.
22. Zhu J, et al. (2003) Allowed N-glycosylation sites on the Kv1.2 potassium channel S1-S2 linker: implications for linker secondary structure and the glycosylation effect on channel function. *Biochem J* 375(Pt 3):769–775.
23. Zhu J, et al. (2009) The Kv1.2 potassium channel: The position of an N-glycan on the extracellular linkers affects its protein expression and function. *Brain Res* 1251:16–29.
24. Lewis A, Jogini V, Blachowicz L, Laine M, Roux B (2008) Atomic constraints between the voltage sensor and the pore domain in a voltage-gated K+ channel of known structure. *J Gen Physiol* 131(6):549–561.
25. Ahern CA, Horn R (2004) Specificity of charge-carrying residues in the voltage sensor of potassium channels. *J Gen Physiol* 123(3):205–216.
26. Starace DM, Bezanilla F (2004) A proton pore in a potassium channel voltage sensor reveals a focused electric field. *Nature* 427(6974):548–553.
27. Posson DJ, Selvin PR (2008) Extent of voltage sensor movement during gating of shaker K+ channels. *Neuron* 59(1):98–109.
28. Pathak MM, et al. (2007) Closing in on the resting state of the Shaker K(+) channel. *Neuron* 56(1):124–140.
29. Tao X, Lee A, Limapichat W, Dougherty DA, MacKinnon R (2010) A gating charge transfer center in voltage sensors. *Science* 328(5974):67–73.
30. Zagotta WN, Hoshi T, Dittman J, Aldrich RW (1994) Shaker potassium channel gating II: Transitions in the activation pathway. *J Gen Physiol* 103(2):279–319.
31. Schoppa NE, McCormack K, Tanouye MA, Sigworth FJ (1992) The size of gating charge in wild-type and mutant Shaker potassium channels. *Science* 255(5052):1712–1715.
32. Seoh SA, Sigg D, Papazian DM, Bezanilla F (1996) Voltage-sensing residues in the S2 and S4 segments of the Shaker K+ channel. *Neuron* 16(6):1159–1167.
33. Aggarwal SK, MacKinnon R (1996) Contribution of the S4 segment to gating charge in the Shaker K+ channel. *Neuron* 16(6):1169–1177.
34. Ma J (2005) Usefulness and limitations of normal mode analysis in modeling dynamics of biomolecular complexes. *Structure* 13:373–380.